https://doi.org/10.1070/QEL16213

Simulation of an intracavity *Q*-switched optical parametric oscillator using rate equations

A. Keshavarz, S. Samimi

Abstract. **Based on rate equations we have refined the model of an intracavity *Q*-switched optical parametric oscillator (IOPO) by taking into account the influence of self-Raman stimulated scattering. The rate equations are solved and analysed in the plane-wave approximation for a Gaussian spatial beam distribution profile under various conditions. The spatial rate equations are also solved numerically for a beam with a field distribution of the TEM_{00} mode. The numerical analysis shows that stimulated self-Raman scattering leads to a decrease in the output signal power and an increase in the signal pulse width. This model allows one to predict that the output signal power can be increased with increasing ratio of Raman to fundamental photon lifetimes. This suggests a practical method for determining the self-Raman gain coefficient experimentally. In addition, a multi-pulse process for the signal beam of the IOPO can be regenerated by the presented model. However, in comparison with the previous research, the presented model is more accurate and allows one to design and optimise single-resonator IOPOs.**

Keywords: *intracavity optical parametric oscillator, self-Raman stimulated scattering.*

1. Introduction

Tunable eye-safe mid-IR lasers find numerous applications in spectroscopy, range finders, military equipment, etc. However, it is difficult to construct a laser source which is tunable in the eye-safe band from a conventional gain medium. In recent years, intracavity optical parametric oscillators (IOPOs) have been developed to provide practical tunable laser sources in the eye-safe band using temperature and quasi-phase-matching techniques [1–5]. A successful theoretical model which describes characteristics of IOPOs in the pulsed regime has been developed by introducing a system of rate equations [6]. The output characteristics of KTA IOPOs have been studied theoretically and the influence of output coupling has been investigated using rate equations in the plane-wave approximation [7–9]. A *Q*-switched Nd:YAG/KTA IOPO has been studied theoretically using spatial rate equations [10]. The design and operation of a solid-state Raman laser has been presented by Pask [11]. Intracavity Raman lasers have been modelled using the system of rate equations [12–17]. However, some laser crystals are characterised by simulated self-Raman scattering (for example, $Nd:YVO_4$ and Nd:GdVO [18, 19]), which prevents a significant part of fundamental photons from reaching the nonlinear crystal, because these photons are re-absorbed and converted to Raman photons which do not satisfy the phase-matching condition in the nonlinear crystal.

Because the self-Raman scattering effect has not been considered in previous studies of IOPO systems, we have included it into our consideration. We have also analysed the rate equations and have numerically investigated the output signal power, pulse width and pulse shape.

A. Keshavarz, S. Samimi Department of Physics, Shiraz University of Technology, Shiraz, Iran; e-mail: keshavarz@sutech.ac.ir

Received 26 September 2016
Kvantovaya Elektronika **47** (3) 280–284 (2017)
Submitted in English

2. Experimental setup

A schematic of a conventional IOPO is shown in Fig. 1. In this setup, the fundamental beam, which is amplified by the gain medium, propagates in the cavity formed by mirrors M1 and M2. Mirror M3 has high transmission at the fundamental wavelength and high reflection at the signal wavelength. Output coupler M2 has partial transmission at the signal wavelength because some of the signal energy should exit from the cavity, formed by M1 and M2, as the IOPO output. In other word, the signal wave is an intrinsic wave in the cavity which is formed by M3 and M2. In this single-cavity IOPO, all optical elements are transparent for the idler wave.

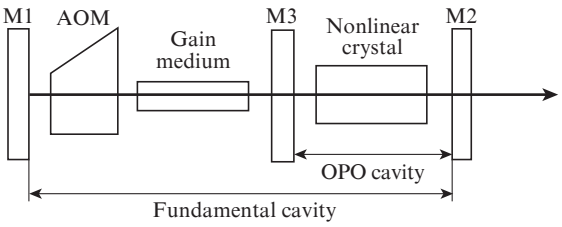

Figure 1. Schematic of an intracavity optical parametric oscillator [7, 20].

3. Theoretical model

By taking self-Raman scattering into account, the most general rate equations [6, 12] for an actively *Q*-switched IOPO can be generalised as:

$$\frac{\mathrm{d}n(r,z,t)}{\mathrm{d}t} = -\gamma c\sigma n(r,z,t)\phi_1(r,z,t), \tag{1}$$

$$\int_{C_1} \frac{\mathrm{d}\phi_1(r,z,t)}{\mathrm{d}t}\,\mathrm{d}V = \int_{LC} c\sigma\phi_1(r,z,t)n(r,z,t)\,\mathrm{d}V$$

$$-\int_{\mathrm{LC}} c\sigma_{\mathrm{r}}\phi_{\mathrm{l}}(r,z,t)\phi_{\mathrm{r}}(r,z,t)\,\mathrm{d}V$$

$$-\int_{\mathrm{NLC}} c\sigma_{\mathrm{nl}}\phi_{\mathrm{ls}}(r,z,t)\phi_{\mathrm{s}}(r,z,t)\,\mathrm{d}V$$

$$-\frac{1}{\tau_{\mathrm{l}}}\int_{C_{\mathrm{l}}}\phi_{\mathrm{l}}(r,z,t)\,\mathrm{d}V, \tag{2}$$

$$\int_{\mathrm{C_2}}\frac{\mathrm{d}\phi_{\mathrm{s}}(r,z,t)}{\mathrm{d}t}\,\mathrm{d}V=\int_{\mathrm{NLC}} c\sigma_{\mathrm{nl}}\phi_{\mathrm{s}}(r,z,t)\phi_{\mathrm{ls}}(r,z,t)\,\mathrm{d}V$$

$$-\frac{1}{\tau_{\mathrm{s}}}\int_{\mathrm{C_2}}\phi_{\mathrm{s}}(r,z,t)\,\mathrm{d}V, \tag{3}$$

$$\int_{\mathrm{C_3}}\frac{\mathrm{d}\phi_{\mathrm{r}}(r,z,t)}{\mathrm{d}t}\,\mathrm{d}V=\int_{\mathrm{LC}} c\sigma_{\mathrm{r}}\phi_{\mathrm{l}}(r,z,t)\phi_{\mathrm{r}}(r,z,t)\,\mathrm{d}V$$

$$-\frac{1}{\tau_{\mathrm{r}}}\int_{\mathrm{C_3}}\phi_{\mathrm{r}}(r,z,t)\,\mathrm{d}V+k_{\mathrm{sp}}\int_{\mathrm{C_3}}\phi_{\mathrm{l}}(r,z,t)\,\mathrm{d}V. \tag{4}$$

Equation (1) is the rate equation for the population inversion and equations (2), (3) and (4) are the rate equations for fundamental laser, signal and Raman photons, respectively. In equation (2), we have introduced the second term to take the influence of self-Raman scattering into account, while equation (4) has been introduced for the description of generation of Raman photons.

In equations (1)–(4), γ is the inversion reduction factor of the gain medium; $n(r,z,t)$ is the population inversion density; $\phi_{\mathrm{l}}(r,z,t)$, $\phi_{\mathrm{s}}(r,z,t)$ and $\phi_{\mathrm{r}}(r,z,t)$ are the laser, signal and Raman photon densities, respectively; $\phi_{\mathrm{ls}}(r,z,t)$ is the fundamental photon density in the nonlinear crystal; $\mathrm{C_1}$, $\mathrm{C_2}$, $\mathrm{C_3}$, LC and NLC denote the spatial integral area in the fundamental cavity, Raman cavity, OPO cavity, laser crystal and nonlinear crystal, respectively; c is the speed of light in vacuum; σ is the stimulated emission cross section of the laser medium; k_{sp} is the spontaneous Raman scattering factor; and τ_{l}, τ_{r} and τ_{s} are the cavity lifetimes of fundamental, Raman and signal photons, respectively, defined as:

$$\tau_j=\frac{t_{\mathrm{r}j}}{L_j+\ln(1/R_j)},\quad j=\mathrm{l,\ r,\ s}. \tag{5}$$

Here, $t_{\mathrm{r}j}$, L_j and R_j are the lifetimes of the photon in the cavity, the round-trip intrinsic loss and the output coupler reflectivity, respectively. Subscripts l, r and s denote the fundamental, Raman and signal photons, respectively.

The parameters σ_{r} and σ_{nl} are the effective cross sections of Raman and nonlinear process which are defined as [7, 12]:

$$\sigma_{\mathrm{r}}=gc\hbar\omega_{\mathrm{r}}, \tag{6}$$

$$\sigma_{\mathrm{nl}}=\frac{\hbar\omega_{\mathrm{l}}\omega_{\mathrm{s}}\omega_{\mathrm{id}}d_{\mathrm{eff}}^2 l_{\mathrm{nl}}}{\varepsilon_0 c^2 n_{\mathrm{l}}^2 n_{\mathrm{s}}^2 n_{\mathrm{id}}}\left(1-\frac{\alpha_{\mathrm{id}}l_{\mathrm{nl}}}{3}\right), \tag{7}$$

where g is the Raman gain coefficient of the gain medium; ω_{r} is the circular frequency of Raman photons; $\hbar=h/(2\pi)$; h is Plank's constant; ω_{l}, ω_{s} and ω_{id} are the circular frequencies of fundamental, signal and idler photons; d_{eff} is the effective nonlinear coefficient of interaction; l_{nl} is the nonlinear crystal length; α_{id} is the absorption coefficient at the idler wavelength; ε_0 is the dielectric constant of the vacuum; and n_{l}, n_{s} and n_{id} are the average refractive indices at the fundamental, signal and idler wavelengths, respectively.

3.1. Rate equations in the plane-wave approximation

In the plane-wave approximation the population inversion and photons densities are only time-depend. However, in the plane-wave approximation, the rate equations can be modified as:

$$\frac{\mathrm{d}n(t)}{\mathrm{d}t}=-\gamma c\sigma n(t)\phi_{\mathrm{l}}(t), \tag{8}$$

$$\frac{\mathrm{d}\phi_{\mathrm{l}}(t)}{\mathrm{d}t}=c\sigma\frac{l_{\mathrm{lc}}}{l_{\mathrm{f}}}n(t)\phi_{\mathrm{l}}(t)-c\sigma_{\mathrm{r}}\frac{l_{\mathrm{lc}}}{l_{\mathrm{f}}}\phi_{\mathrm{l}}(t)\phi_{\mathrm{r}}(t)$$

$$-c\sigma_{\mathrm{nl}}\frac{l_{\mathrm{nl}}}{l_{\mathrm{f}}}\phi_{\mathrm{l}}(t)\phi_{\mathrm{s}}(t)-\frac{1}{\tau_{\mathrm{l}}}\phi_{\mathrm{l}}(t), \tag{9}$$

$$\frac{\mathrm{d}\phi_{\mathrm{s}}(t)}{\mathrm{d}t}=c\sigma_{\mathrm{nl}}\frac{l_{\mathrm{nl}}}{l_{\mathrm{OPO}}}\phi_{\mathrm{l}}(t)\phi_{\mathrm{s}}(t)-\frac{1}{\tau_{\mathrm{s}}}\phi_{\mathrm{s}}(t), \tag{10}$$

$$\frac{\mathrm{d}\phi_{\mathrm{r}}(t)}{\mathrm{d}t}=c\sigma_{\mathrm{r}}\frac{l_{\mathrm{lc}}}{l_{\mathrm{f}}}\phi_{\mathrm{l}}(t)\phi_{\mathrm{r}}(t)-\frac{1}{\tau_{\mathrm{r}}}\phi_{\mathrm{r}}(t)+k_{\mathrm{sp}}\phi_{\mathrm{l}}(t). \tag{11}$$

Here, l_{f} and l_{OPO} are the optical lengths of the fundamental and OPO cavity, respectively, and l_{lc} is the laser crystal length.

The threshold population inversion density for the fundamental laser can be obtained by setting $\mathrm{d}\phi_{\mathrm{l}}(t)/\mathrm{d}t$, $\phi_{\mathrm{l}}(t)$, $\phi_{\mathrm{s}}(t)$ and $\phi_{\mathrm{r}}(t)$ equal to zero in equation (9). Then,

$$n_{\mathrm{th}}=\frac{L_{\mathrm{l}}+\ln(1/R_{\mathrm{l}})}{2\sigma l_{\mathrm{lc}}}. \tag{12}$$

The normalised rate equations can be obtained if we introduce the parameters,

$$\Phi_j(\tau)=\frac{2\gamma\sigma l_{\mathrm{lc}}}{\ln(1/R_{\mathrm{l}})+L_{\mathrm{l}}}\phi_j(t),\quad j=\mathrm{l,\ s,\ r}, \tag{13}$$

$$\tau=\frac{t}{t_{\mathrm{rl}}}[\ln(1/R_{\mathrm{l}})+L_{\mathrm{l}}], \tag{14}$$

$$N(\tau)=n/n_{\mathrm{th}}, \tag{15}$$

$$K_{\mathrm{sp}}=\frac{t_{\mathrm{rl}}}{\ln(1/R_{\mathrm{l}})+L_{\mathrm{l}}}k_{\mathrm{sp}}. \tag{16}$$

By substituting these parameters into rate equations (8)–(11), we obtain

$$\frac{\mathrm{d}N}{\mathrm{d}\tau}=-N\Phi_{\mathrm{l}}, \tag{17}$$

$$\frac{\mathrm{d}\Phi_{\mathrm{l}}}{\mathrm{d}\tau}=N\Phi_{\mathrm{l}}-M_{\mathrm{r}}\Phi_{\mathrm{l}}\Phi_{\mathrm{r}}-M_{\mathrm{s}}\Phi_{\mathrm{l}}\Phi_{\mathrm{s}}-\Phi_{\mathrm{l}}, \tag{18}$$

$$\frac{\mathrm{d}\Phi_{\mathrm{s}}}{\mathrm{d}\tau}=G\Phi_{\mathrm{l}}\Phi_{\mathrm{s}}-K_{\mathrm{s}}\Phi_{\mathrm{s}}, \tag{19}$$

$$\frac{\mathrm{d}\Phi_{\mathrm{r}}}{\mathrm{d}\tau}=M_{\mathrm{r}}\Phi_{\mathrm{l}}\Phi_{\mathrm{r}}-K_{\mathrm{r}}\Phi_{\mathrm{r}}+K_{\mathrm{sp}}\Phi_{\mathrm{l}}. \tag{20}$$

Here,

$$M_{\mathrm{r}}=\frac{\sigma_{\mathrm{r}}l_{\mathrm{lc}}}{\gamma\sigma l_{\mathrm{f}}},\quad M_{\mathrm{s}}=\frac{\sigma_{\mathrm{nl}}l_{\mathrm{nl}}}{\gamma\sigma l_{\mathrm{f}}},\quad G=\frac{M_{\mathrm{s}}l_{\mathrm{f}}}{l_{\mathrm{OPO}}},$$

and loss ratios are given by

$$K_j = \frac{\ln(1/R_j) + L_j}{\ln(1/R_l) + L_l},\ j = \mathrm{s, r}. \tag{21}$$

Rate equations (17)–(20) describe IOPO characteristics in the plane-wave approximation.

3.2. Space-dependent rate equations

To take the beam spatial distribution into account, fundamental, Raman and signal beams are assumed to have a Gaussian spatial profile (TEM_{00} mode), which is given as

$$\phi_j(r,t) = \phi_j(t)\exp\left(\frac{-2r^2}{w_j^2}\right),\ j = \mathrm{l, s, r}. \tag{22}$$

For the fundamental photon density in the nonlinear crystal, $\phi_{ls}(r,t)$, we set

$$\phi_{ls}(r,t) = \phi_{ls}(t)\exp\left(\frac{-2r^2}{w_{ls}^2}\right), \tag{23}$$

where $\phi_{ls}(t)$ is related to $\phi_l(t)$ by the law of conservation of the photon flux:

$$w_l^2\phi_l(t) = w_{ls}^2\phi_{ls}(t). \tag{24}$$

Here, w_{ls} is the fundamental beam diameter in the nonlinear crystal. For end-pumped laser diodes with a four-level gain medium, it is reasonable to assume that the initial population inversion has a Gaussian spatial profile [21]:

$$n(r) = n(0)\exp\left(\frac{-2r^2}{w_p^2}\right), \tag{25}$$

where $n(0)$ is the initial population inversion density on the gain medium axis and w_p is the diameter of the pump beam in the gain medium. By using spatial rate equations, the threshold initial population inversion is modified to

$$n_{th} = \frac{L_l + \ln(1/R_l)}{2\sigma l_{lc}}\left(1 + \frac{w_l^2}{w_p^2}\right). \tag{26}$$

We introduce the notations

$$\beta = \left(1 + \frac{w_l^2}{w_p^2}\right)^{-1},\quad M_{rs} = M_r\left(1 + \frac{w_l^2}{w_r^2}\right)^{-1},\quad M_{ss} = M_s\left(1 + \frac{w_{ls}^2}{w_s^2}\right)^{-1},$$

$$G_s = M_{ss}\frac{l_f}{l_{OPO}}\frac{w_l^2}{w_s^2},\quad M_{rl} = M_{rs}\frac{w_l^2}{w_r^2},\quad K_{sps} = K_{sp}\frac{w_l^2}{w_r^2}.$$

Then, the modified normalised spatial rate equations have the form

$$\frac{d\Phi_l(\tau)}{d\tau} = \Phi_l(\tau)N(0)\int_0^1 \exp[-F(\tau)y^\beta]dy - M_{rs}\Phi_l(\tau)\Phi_r(\tau) - M_{ss}\Phi_l(\tau)\Phi_s(\tau) - \Phi_l(\tau), \tag{27}$$

$$\frac{d\Phi_s(\tau)}{d\tau} = G_s\Phi_l(\tau)\Phi_s(\tau) - K_s\Phi_s(\tau), \tag{28}$$

$$\frac{d\Phi_r(\tau)}{d\tau} = M_{rl}\Phi_l(\tau)\Phi_r(\tau) + K_{sps}\Phi_l(\tau) - K_r\Phi_r(\tau), \tag{29}$$

$$\frac{dF(\tau)}{d\tau} = \Phi_l(\tau). \tag{30}$$

Equations (27)–(30) are the normalised spatial rate equations which describe the characteristics of IOPOs.

4. Numerical analysis

In this section, rate equations (17)–(20) and (27)–(30) are solved numerically. To analyse the spatial rate equations numerically, we must first determine the ratio of the fundamental laser mode diameter to the pump mode diameter, w_l/w_p. We assume in this case that the maximum spatial beam overlapping takes place at $w_l/w_p = 1$.

Figure 2 shows the time dependence of the photon density in the plane-wave approximation for two lifetimes of Raman photons. One can see that the signal photon density increases with increasing relative lifetime of Raman photons.

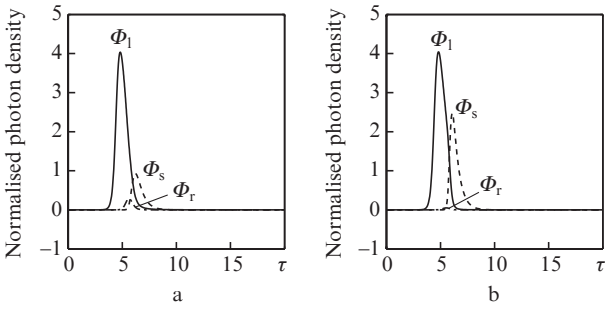

Figure 2. Densities of fundamental, signal and Raman photons as functions of time in the plane-wave approximation at K_r = (a) 5 and (b) 7 [$N(0) = 7$, $M_r = 3$, $M_s = 2$, $G = 6$, $K_{sp} = 10^{-3}$, $K_s = 2$].

Figure 3 shows similar dependences calculated by using the spatial rate equations in which the condition of full spatial overlapping is satisfied ($w_l/w_p = 1$). From the comparison of Figs 2 and 3 one can conclude that the pulses, which are calculated by using the rate equations in the plane-wave approximation, are narrower than the pulses which are calculated by the equations taking into account the spatial profiles of the beams.

The signal pulse width as a function of the Raman normalised gain coefficient is presented in Fig. 4. One can see from the figure that the signal pulse width has a maximum

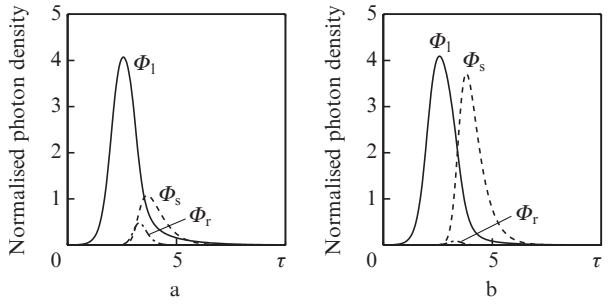

Figure 3. Densities of fundamental, signal and Raman photons as functions of time for Gaussian beams at K_r = (a) 5 and (b) 7 [$N(0) = 5.2$, $M_{rs} = 2.85$, $M_{ss} = 0.5$, $G_s = 2.6$, $M_{rl} = 2.85$, $K_{sps} = 10^{-3}$, $K_s = 2$].

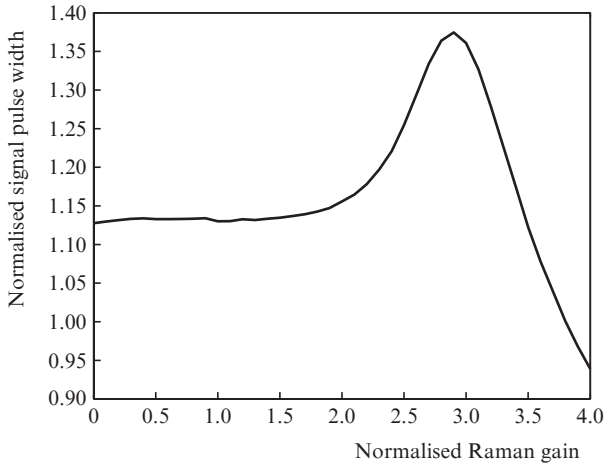

Figure 4. Pulse width as a function of normalised spatial Raman gain coefficient at $N(0) = 5.2$, $M_{ss} = 0.5$, $G_s = 2.6$, $K_{sps} = 10^{-3}$, $K_s = 2$, and $K_r = 5$.

value. The Raman gain coefficient of the crystal can be determined using this maximum value in the following way.

Step 1: In Eqns (27) and (29) the parameters M_{rs}, M_{rl} and K_{sps} are the functions of fundamental-to-Raman beam diameter ratio (w_l/w_r). Therefore, in the fixed setup the pulse width can be changed by varying w_l/w_r. The parameter $(w_l/w_r)_{max}$ corresponding to a pulse with a maximum width can be obtained experimentally.

Step 2: The normalised Raman gain $(M_{rs})_{max}$, at which a signal pulse of maximum width is formed, can be calculated by the presented model.

Step 3: Finally, the Raman gain coefficient of the laser crystal can be determined by:

$$g = \gamma\sigma \frac{l_f}{c\hbar\omega_r l_{lc}} \left[1 + \left(\frac{w_l}{w_r}\right)^2_{max}\right] (M_{rs})_{max}. \qquad (31)$$

Figure 5 shows the normalised signal pulse widths calculated with self-Raman scattering and without it as functions of the initial population inversion. A longer pulse width is obtained if self-Raman scattering is taken into account.

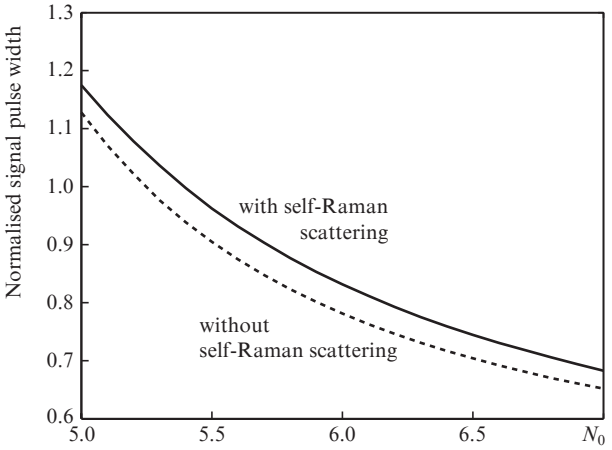

Figure 5. Widths of a signal pulse as functions of the normalised initial population inversion at $M_{rs} = 2.85$, $M_{ss} = 0.5$, $G_s = 2.6$, $K_{sps} = 10^{-3}$, $K_s = 2$, and $K_r = 5$.

The signal output power is proportional to the integral of the normalised signal photon density in the normalised time [15]. Therefore, Fig. 6 shows the result of the integration of the normalised signal photon density in the normalised time $\Phi_{s\,integ}$ as a function of the normalised initial population inversion. The self-Raman scattering causes the $\Phi_{s\,integ}$ decrease, because a large number of fundamental photons are re-absorbed in the gain medium, are converted to the Raman photons due to Raman scattering, and do not participate in the nonlinear interaction with the nonlinear crystal.

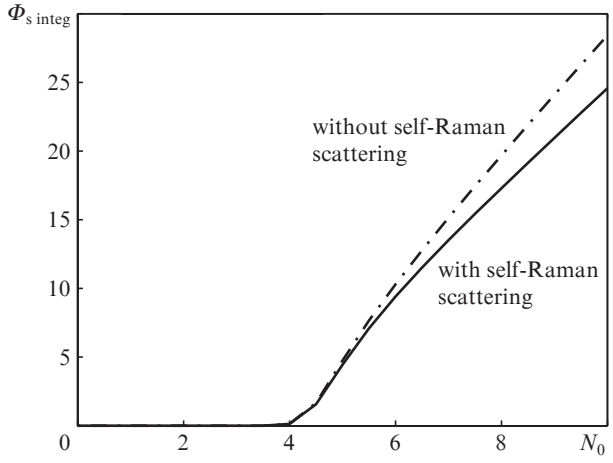

Figure 6. Dependence of $\Phi_{s\,integ}$ on the normalised initial population inversion at $M_{rs} = 2.85$, $M_{ss} = 0.5$, $G_s = 2.6$, $K_{sps} = 10^{-3}$, $K_s = 2$, and $K_r = 5$.

The presented model allows one to describe multi-pulse regimes, which have been observed in the experimental research [22–25]. Figures 7 and 8 show the time dependences of the normalised population inversion and pulse shapes for a model setup in which $Nd:YVO_4$ and KTP crystals are used as laser and nonlinear gain media, respectively.

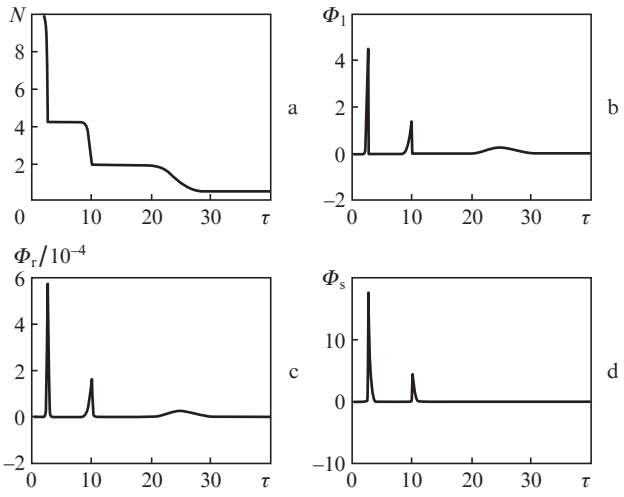

Figure 7. Multi-pulse generation characteristics for the $Nd:YVO_4$ laser crystal and KTP nonlinear crystal in the plane-wave approximation: (a) normalised population inversion as well as (b) laser, (c) Raman and (d) signal photon densities.

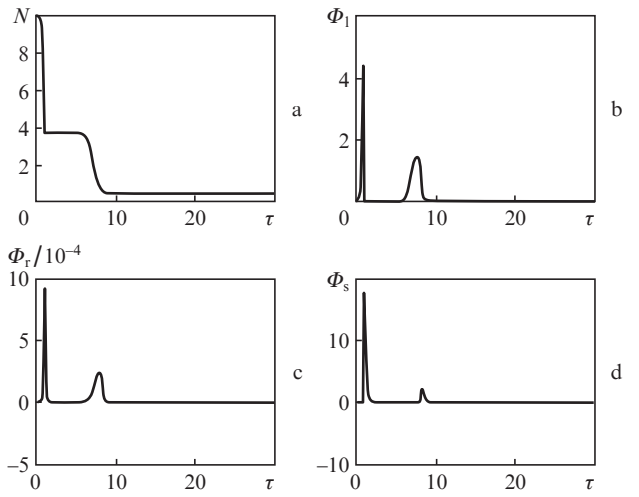

Figure 8. Multi-pulse generation characteristics for the Nd:YVO_4 laser crystal and KTP nonlinear crystal for Gaussian beams: (a) normalised population inversion as well as (b) laser, (c) Raman and (d) signal photon densities.

5. Conclusions

Self-Raman scattering plays an important role in the IOPO with such gain media as Nd:YVO_4, because an intrinsic self-Raman gain coefficient arises in these media. To reduce the influence of self-Raman scattering, the Raman loss ratio must be chosen as big as possible which can be done by choosing an appropriate output coupler at the Raman wavelength. A practical method is suggested to determine the Raman gain coefficient by analysing spatial rate equations. A wider pulse width is shown to result from self-Raman scattering of the gain medium. In this case, the output signal power is reduced as a number of fundamental photons are converted to the Raman photons which do not participate in the interaction with the nonlinear crystal. The multi-pulse generation can be studied theoretically by the presented model. In comparison with the previous model, the model in question provides more accurate calculation results, which are needed to design and optimise IOPO systems.

References

1. Ding X., Sheng Q., Chen N., Yu X.-Y., Wang R., Zhang H., Wen W.-Q., Wang P., Yao J.-Q. *Chin. Phys. B*, **18** (10), 4314 (2009).
2. Wan Y., Zeng Q.-Y., Zhu D.-Y., Han K., Li T., Han H., Yu S.-F., Su X.-Z. *Chin. Phys.*, **13** (9), 1402 (2004).
3. Liu J.-L., Liu Q., Li H., Li P., Zhang K.-S. *Chin. Phys. B*, **20** (11), 114215 (2011).
4. Lin X.-C., Kong Y.-P., Zhang Y., Zhang J., Yao A.-Y., Bi Y., Sun Z.-P., Cui D.-F., Wu Li R.-N., Ling A., et al. *Chin. Phys.*, **13** (7), 1042 (2004).
5. Ding X., Yao J.-q., Yu Y.-z., Yu X.-y., Xu J.-j., Zhang G.-y. *Chin. Phys.*, **10** (8), 725 (2001).
6. Debuisschert T., Raffy J., Pocholle J.-P., Papuchon M. *J. Opt. Soc. Am. B*, **13** (7), 1569 (1996).
7. Bai F., Wang Q., Liu Zh., Zhang X., Wan X., Lan W., Jin G., Tao X., Sun Y. *Opt. Express*, **20** (2), 807 (2012).
8. Li G., Wang Q., Bai F., Gao Y., Zheng G., Zhao Y., Chen K. *Laser Phys.*, **23** (2), 025402 (2013).
9. Huang Y.P., Huang Y.J., Cho C.Y., Chen Y.F. *Opt. Express*, **21** (6), 7583 (2013).
10. Liu Z., Wang Q., Zhang X., Chang J., Wang H., Fan S., Sun W., Jin G., Tao X., Zhang S., et al. *Appl. Phys. B*, **92** (1), 37 (2008).
11. Pask H.M.I. *Prog. Quantum Electron.*, **27** (1), 3 (2003).
12. Bai F., Wang Q., Liu Zh., Zhang X., Wan X., Lan W., Jin G., Zhang H. *IEEE J. Quantum Electron.*, **48** (5), 581 (2012).
13. Kazzaz A., Ruschin Sh., Shoshan I., Ravnitsky G. *IEEE J. Quantum Electron.*, **30** (12), 3017 (1994).
14. Ding Sh., Zhang X., Wang Q., Chang J., Wang Sh., Liu Y. *IEEE J. Quantum Electron.*, **43** (8), 722 (2007).
15. Zhang X., Zhao Sh., Wang Q., Ozygus B., Weber H. *J. Opt. Soc. Am. B*, **17** (7), 1166 (2000).
16. Loiko Yu.V., Demidovich A.A., Burakevich V.V., Voitovich A.P. *J. Opt. Soc. Am. B*, **22** (11), 2450 (2005).
17. Murray J.T., Austin W.L., Powell R.C. *Opt. Mater.*, **11** (4), 353 (1999).
18. Ding Sh., Zhang X., Wang Q., Su F., Jia P., Li Sh., Fan Sh., Chang J., Zhang S., Liu Zh. *IEEE J. Quantum Electron.*, **42** (9), 927 (2006).
19. Chen Y.F. *Opt. Lett.*, **29** (16), 1915 (2004).
20. Huang H.T., He J.L., Dong X.L., Zuo C.H., Zhang B.T., Qiu G., Liu Z.K. *Appl. Phys. B*, **90** (1), 43 (2008).
21. Zhang X., Zhao Sh., Wang Q., Ozygus B., Weber H. *IEEE J. Quantum Electron.*, **35** (12), 1912 (1999).
22. Dabu R., Fenic C., Stratan A. *Appl. Opt.*, **40** (24), 4334 (2001).
23. Chen Y.F., Chen S.W., Tsai S.W., Lan Y.P. *Appl. Phys. B*, **77** (5), 505 (2003).
24. Yang J.-F., Zhang B.-T., He J.-L., Huang H.-T., Dong X.-L., Xu J.-L., Zuo C.-H., Zhao S., Yang X.-Q., Qiu G., et al. *Appl. Phys. B*, **98** (1), 49 (2010).
25. Cho C.Y., Chen Y.C., Huang Y.P., Huang Y.J., Su K.W., Chen Y.F. *Opt. Express*, **22** (7), 7625 (2014).